Chapter 4

Laser Dynamics (single-mode)

Before we start to look into the dynamics of a multi-mode laser, we should recall the technically important regimes of operation of a "single-mode" laser. The term "single-mode" is set in apostrophes, since it doesn't have to be really single-mode. There can be several modes running, for example due to spatial holeburning, but in an incoherent fashion, so that only the average power of the beam matters. For a more detailed account on single-mode laser dynamics and Q-Switching the following references are recommended [1][3][16][4][5].

4.1 Rate Equations

In section 2.5, we derived for the interaction of a two-level atom with a laser field propagating to the right the equations of motion (2.171) and (2.172), which are given here again:

$$\left(\frac{\partial}{\partial z}+\frac{1}{v_g}\frac{\partial}{\partial t}\right)A(z,t) = \frac{N\hbar}{4T_2E_s}w\left(z,t\right)A(z,t), \tag{4.1}$$

$$\dot{w} = -\frac{w-w_0}{T_1}+\frac{\left|A(z,t)\right|^2}{E_s}w(z,t) \tag{4.2}$$

where T_1 is the energy relaxation rate, v_g the group velocity in the host material where the two level atoms are embedded, $E_s = I_sT_1$, the saturation fluence $[J/cm^2]$, of the medium.and I_s the saturation intensity according to

Eq.(2.145)

$$I_s = \left[\frac{2T_1 T_2 Z_F}{\hbar^2} \frac{\left| \vec{M} \hat{\vec{E}} \right|^2}{\left| \hat{\vec{E}} \right|^2} \right]^{-1},$$

which relates the saturation intensity to the microscopic parameters of the transition like longitudinal and transversal relaxation rates as well as the dipole moment of the transition.

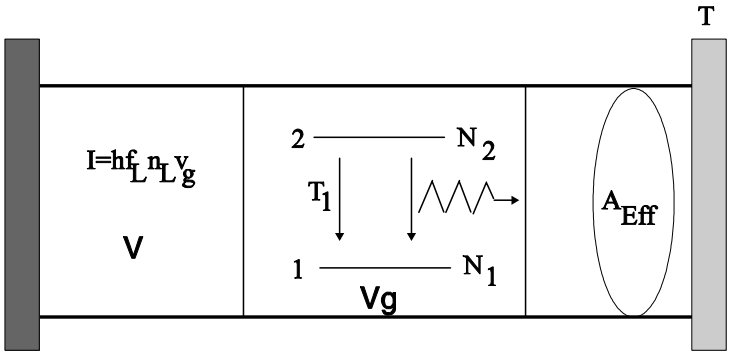

Figure 4.1: Rate equations for the two-level atom

In many cases it is more convenient to normalize (4.1) and (4.2) to the populations in level e and g or 2 and 1, respectively, N_2 and N_1, and the density of photons, n_L, in the mode interacting with the atoms and traveling at the corresponding group velocity, v_g, see Fig. 4.1. The intensity I in a mode propagating at group velocity v_g with a mode volume V is related to the number of photons N_L stored in the mode with volume V by

$$I = hf_L \frac{N_L}{2^* V} v_g = \frac{1}{2^*} hf_L n_L v_g, \tag{4.3}$$

where hf_L is the photon energy. $2^* = 2$ for a linear laser resonator (then only half of the photons are going in one direction), and $2^* = 1$ for a ring laser. In this first treatment we consider the case of space-independent rate equations, i.e. we assume that the laser is oscillating on a single mode and pumping and mode energy densities are uniform within the laser material. With the interaction cross section σ defined as

$$\sigma = \frac{hf_L}{2^* I_s T_1}, \tag{4.4}$$

and multiplying Eq. (**??**) with the number of atoms in the mode, we obtain

$$\frac{d}{dt}(N_2 - N_1) = -\frac{(N_2 - N_1)}{T_1} - \sigma\,(N_2 - N_1)\,v_g n_L + R_p \tag{4.5}$$

Note, $v_g n_L$ is the photon flux, thus σ is the stimulated emission cross section between the atoms and the photons. R_p is the pumping rate into the upper laser level. A similar rate equation can be derived for the photon density

$$\frac{d}{dt}n_L = -\frac{n_L}{\tau_p} + \frac{l_g}{L}\frac{\sigma v_g}{V_g}\left[N_2\,(n_L + 1) - N_1 n_L\right]. \tag{4.6}$$

Here, τ_p is the photon lifetime in the cavity or cavity decay time and the one in Eq.(4.6) accounts for spontaneous emission which is equivalent to stimulated emission by one photon occupying the mode. V_g is the volume of the active gain medium. For a laser cavity with a semi-transparent mirror with transmission T, producing a small power loss $2l = -\ln(1-T) \approx T$ (for small T) per round-trip in the cavity, the cavity decay time is $\tau_p = 2l/T_R$, if $T_R = 2^*L/c_0$ is the roundtrip-time in linear cavity with optical length $2L$ or a ring cavity with optical length L. The optical length L is the sum of the optical length in the gain medium $n_g^{group} l_g$ and the remaining free space cavity length l_a. Internal losses can be treated in a similar way and contribute to the cavity decay time. Note, the decay rate for the inversion in the absence of a field, $1/T_1$, is not only due to spontaneous emission, but is also a result of non radiative decay processes. See for example the four level system shown in Fig. 4.2. In the limit, where the populations in the third and first level are zero, because of fast relaxation rates, i.e. T_{32}, $T_{10} \to 0$, we obtain

$$\frac{d}{dt}N_2 = -\frac{N_2}{\tau_L} - \sigma v_g N_2 n_L + R_p \tag{4.7}$$

$$\frac{d}{dt}n_L = -\frac{n_L}{\tau_p} + \frac{l_g}{L}\frac{\sigma v_g}{V_g}N_2\,(n_L + 1)\,. \tag{4.8}$$

where $\tau_L = T_{21}$ is the lifetime of the upper laser level. Experimentally, the photon number and the inversion in a laser resonator are not

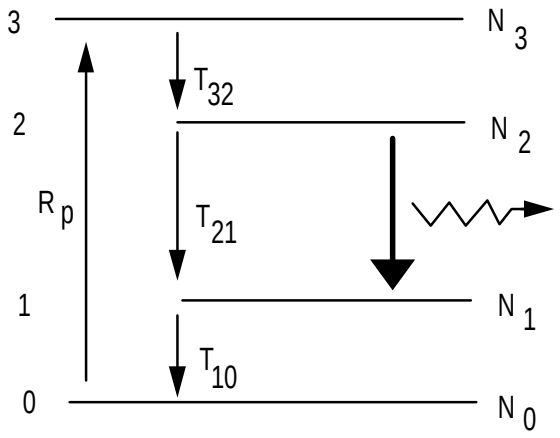

Figure 4.2: Vier-Niveau-Laser

very convenient quantities, therefore, we normalize both equations to the round-trip amplitude gain $g = \frac{l_g}{L}\frac{\sigma v_g}{2V_g}N_2 T_R$ experienced by the light and the circulating intracavity power $P = I \cdot A_{eff}$

$$\frac{d}{dt}g = -\frac{g - g_0}{\tau_L} - \frac{gP}{E_{sat}} \tag{4.9}$$

$$\frac{d}{dt}P = -\frac{1}{\tau_p}P + \frac{2g}{T_R}\left(P + P_{vac}\right), \tag{4.10}$$

with

$$E_s = I_s A_{eff}\tau_L = \frac{hf_L}{2^*\sigma} \tag{4.11}$$

$$P_{sat} = E_{sat}/\tau_L \tag{4.12}$$

$$P_{vac} = hf_L v_g/2^* L = hf_L/T_R \tag{4.13}$$

$$g_0 = \frac{2^* v_g R_p}{2A_{eff}c_0}\sigma\tau_L, \tag{4.14}$$

the small signal round-trip gain of the laser. Note, the factor of two in front of gain and loss is due to the fact, the g and l are gain and loss with respect to amplitude. Eq.(4.14) elucidates that the figure of merit that characterizes the small signal gain achievable with a certain laser material is the $\sigma\tau_L$-product.

Laser Medium	Wave-length $\lambda_0(n\text{m})$	Cross Section σ (cm^2)	Upper-St. Lifetime τ_L (μs)	Linewidth $\Delta f_{FWHM} = \frac{2}{T_2}$(THz)	Typ	Refr. index n
Nd^{3+}:YAG	1,064	$4.1 \cdot 10^{-19}$	1,200	0.210	H	1.82
Nd^{3+}:LSB	1,062	$1.3 \cdot 10^{-19}$	87	1.2	H	1.47 (ne)
Nd^{3+}:YLF	1,047	$1.8 \cdot 10^{-19}$	450	0.390	H	1.82 (ne)
Nd^{3+}:YVO_4	1,064	$2.5 \cdot 10^{-19}$	50	0.300	H	2.19 (ne)
Nd^{3+}:glass	1,054	$4 \cdot 10^{-20}$	350	3	H/I	1.5
Er^{3+}:glass	1,55	$6 \cdot 10^{-21}$	10,000	4	H/I	1.46
Ruby	694.3	$2 \cdot 10^{-20}$	1,000	0.06	H	1.76
Ti^{3+}:Al_2O_3	660-1180	$3 \cdot 10^{-19}$	3	100	H	1.76
Cr^{3+}:LiSAF	760-960	$4.8 \cdot 10^{-20}$	67	80	H	1.4
Cr^{3+}:LiCAF	710-840	$1.3 \cdot 10^{-20}$	170	65	H	1.4
Cr^{3+}:LiSGAF	740-930	$3.3 \cdot 10^{-20}$	88	80	H	1.4
He-Ne	632.8	$1 \cdot 10^{-13}$	0.7	0.0015	I	$\sim$1
Ar^+	515	$3 \cdot 10^{-12}$	0.07	0.0035	I	$\sim$1
CO_2	10,600	$3 \cdot 10^{-18}$	2,900,000	0.000060	H	$\sim$1
Rhodamin-6G	560-640	$3 \cdot 10^{-16}$	0.0033	5	H	1.33
semiconductors	450-30,000	$\sim 10^{-14}$	~ 0.002	25	H/I	3 - 4

Table 4.1: Wavelength range, cross-section for stimulated emission, upper-state lifetime, linewidth, typ of lineshape (H=homogeneously broadened, I=inhomogeneously broadened) and index for some often used solid-state laser materials, and in comparison with semiconductor and dye lasers.

The larger this product the larger is the small signal gain g_0 achievable with a certain laser material. Table 4.1

From Eq.(2.145) and (4.4) we find the following relationship between the interaction cross section of a transition and its microscopic parameters like linewidth, dipole moment and energy relaxation rate

$$\sigma = \frac{hf_L}{I_{sat}T_1} = \frac{2T_2}{\hbar^2 Z_F}\frac{|\vec{M}\hat{\vec{E}}|^2}{|\hat{\vec{E}}|^2}.$$

This equation tells us that broadband laser materials naturally do show smaller gain cross sections, if the dipole moment is the same.

4.2 Built-up of Laser Oscillation and Continuous Wave Operation

If $P_{vac} \ll P \ll P_{sat} = E_{sat}/\tau_L$, than $g = g_0$ and we obtain from Eq.(4.10), neglecting P_{vac}

$$\frac{dP}{P} = 2\left(g_0 - l\right)\frac{dt}{T_R} \tag{4.15}$$

or

$$P(t) = P(0)e^{2(g_0-l)\frac{t}{T_R}}. \tag{4.16}$$

The laser power builts up from vaccum fluctuations until it reaches the saturation power, when saturation of the gain sets in within the built-up time

$$T_B = \frac{T_R}{2\left(g_0 - l\right)}\ln\frac{P_{sat}}{P_{vac}} = \frac{T_R}{2\left(g_0 - l\right)}\ln\frac{A_{eff}T_R}{\sigma\tau_L}. \tag{4.17}$$

Some time after the built-up phase the laser reaches steady state, with the saturated gain and steady state power resulting from Eqs.(4.9-4.10), neglecting in the following the spontaneous emission, and for $\frac{d}{dt} = 0$:

$$g_s = \frac{g_0}{1 + \frac{P_s}{P_{sat}}} = l \tag{4.18}$$

$$P_s = P_{sat}\left(\frac{g_0}{l} - 1\right), \tag{4.19}$$

Figure 4.3: Built-up of laser power from spontaneous emission noise.

4.3 Stability and Relaxation Oscillations

How does the laser reach steady state, once a perturbation has occured?

$$g = g_s + \Delta g \tag{4.20}$$
$$P = P_s + \Delta P \tag{4.21}$$

Substitution into Eqs.(4.9-4.10) and linearization leads to

$$\frac{d\Delta P}{dt} = +2\frac{P_s}{T_R}\Delta g \tag{4.22}$$
$$\frac{d\Delta g}{dt} = -\frac{g_s}{E_{sat}}\Delta P - \frac{1}{\tau_{stim}}\Delta g \tag{4.23}$$

where $\frac{1}{\tau_{stim}} = \frac{1}{\tau_L}\left(1 + \frac{P_s}{Psat}\right)$ is the stimulated lifetime. The perturbations decay or grow like

$$\begin{pmatrix} \Delta P \\ \Delta g \end{pmatrix} = \begin{pmatrix} \Delta P_0 \\ \Delta g_0 \end{pmatrix} e^{st}. \tag{4.24}$$

which leads to the system of equations (using $g_s = l$)

$$A\begin{pmatrix} \Delta P_0 \\ \Delta g_0 \end{pmatrix} = \begin{pmatrix} -s & 2\frac{P_s}{T_R} \\ -\frac{T_R}{E_{sat}2\tau_p} & -\frac{1}{\tau_{stim}} - s \end{pmatrix}\begin{pmatrix} \Delta P_0 \\ \Delta g_0 \end{pmatrix} = 0. \tag{4.25}$$

There is only a solution, if the determinante of the coefficient matrix vanishes, i.e.

$$s\left(\frac{1}{\tau_{stim}}+s\right)+\frac{P_s}{E_{sat}\tau_p}=0, \tag{4.26}$$

which determines the relaxation rates or eigen frequencies of the linearized system

$$s_{1/2}=-\frac{1}{2\tau_{stim}}\pm\sqrt{\left(\frac{1}{2\tau_{stim}}\right)^2-\frac{P_s}{E_{sat}\tau_p}}. \tag{4.27}$$

Introducing the pump parameter $r=1+\frac{P_s}{P_{sat}}$, which tells us how often we pump the laser over threshold, the eigen frequencies can be rewritten as

$$\begin{aligned} s_{1/2} &= -\frac{1}{2\tau_{stim}}\left(1\pm j\sqrt{\frac{4\,(r-1)}{r}\frac{\tau_{stim}}{\tau_p}-1}\right), && (4.28)\\ &= -\frac{r}{2\tau_L}\pm j\sqrt{\frac{(r-1)}{\tau_L\tau_p}-\left(\frac{r}{2\tau_L}\right)^2} && (4.29)\end{aligned}$$

There are several conclusions to draw:

- (i): The stationary state $(0, g_0)$ for $g_0 < l$ and (P_s, g_s) for $g_0 > l$ are always stable, i.e. $\mathrm{Re}\{s_i\} < 0$.

- (ii): For lasers pumped above threshold, $r > 1$, the relaxation rate becomes complex, i.e. there are relaxation oscillations

  $$s_{1/2}=-\frac{1}{2\tau_{stim}}\pm j\sqrt{\frac{1}{\tau_{stim}\tau_p}}. \tag{4.30}$$

  with frequency ω_R equal to the geometric mean of inverse stimulated lifetime and photon life time

  $$\omega_R=\sqrt{\frac{1}{\tau_{stim}\tau_p}}. \tag{4.31}$$

  There is definitely a parameter range of pump powers for laser with long upper state lifetimes, i.e. $\frac{r}{4\tau_L}<\frac{1}{\tau_p}$

- If the laser can be pumped strong enough, i.e. r can be made large enough so that the stimulated lifetime becomes as short as the cavity decay time, relaxation oscillations vanish.

The physical reason for relaxation oscillations and later instabilities is, that the gain reacts to slow on the light field, i.e. the stimulated lifetime is long in comparison with the cavity decay time.

Example: diode-pumped Nd:YAG-Laser

$$\begin{aligned} \lambda_0 &= 1064 \text{ nm}, \sigma = 4 \cdot 10^{-20} cm^2,\ A_{eff} = \pi \left(100\mu m \times 150\mu m\right), r = 50 \\ \tau_L &= 1.2\ ms,\ l = 1\%,\ T_R = 10ns \end{aligned}$$

From Eq.(4.4) we obtain:

$$\begin{aligned} I_{sat} &= \frac{hf_L}{\sigma\tau_L} = 3.9\frac{kW}{cm^2},\ P_{sat} = I_{sat}A_{eff} = 1.8\ W,\ P_s = 91.5W \\ \tau_{stim} &= \frac{\tau_L}{r} = 24\mu s,\ \tau_p = 1\mu s, \omega_R = \sqrt{\frac{1}{\tau_{stim}\tau_p}} = 2 \cdot 10^5 s^{-1}. \end{aligned}$$

Figure 4.4 shows the typically observed fluctuations of the output of a solid-state laser with long upperstate life time of several 100 μs in the time and frequency domain.

One can also define a quality factor for the relaxation oscillations by the ratio of imaginary to real part of the complex eigen frequencies 4.29

$$Q = \sqrt{\frac{4\tau_L}{\tau_p}\frac{(r-1)}{r^2}},$$

which can be as large a several thousand for solid-state lasers with long upper-state lifetimes in the millisecond range.

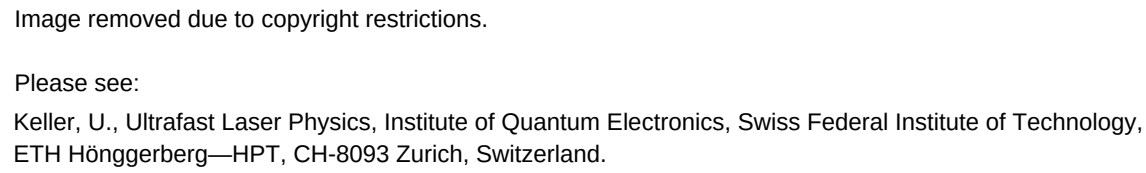

Figure 4.4: Typically observed relaxation oscillations in time and frequency domain.

4.4 Q-Switching

The energy stored in the laser medium can be released suddenly by increasing the Q-value of the cavity so that the laser reaches threshold. This can be done actively, for example by quickly moving one of the resonator mirrors in place or passively by placing a saturable absorber in the resonator [1, 16]. Hellwarth was first to suggest this method only one year after the invention of

Figure 4.5: Gain and loss dynamics of an actively Q-switched laser.

the laser. As a rough orientation for a solid-state laser, the following relation for the relevant time scales is generally valid

$$\tau_L \gg T_R \gg \tau_p. \tag{4.32}$$

4.4.1 Active Q-Switching

Fig. 4.5 shows the principle dynamics of an actively Q-switched laser. The laser is pumped by a pump pulse with a length on the order of the upper-state lifetime, while the intracavity losses are kept high enough, so that the laser can not reach threshold. Therefore, the laser medium acts as an energy storage. The energy only relaxes by spontenous and nonradiative transitions. Then suddenly the intracavity loss is reduced, for example by a rotating cavity mirror. The laser is pumped way above threshold and the light field builts up exponentially with the net gain until the pulse energy comes close to the saturation energy of the gain medium. The gain saturates and is extracted, so that the laser is shut off by the pulse itself.

A typical actively Q-switched pulse is asymmetric: The rise time is proportional to the net gain after the Q-value of the cavity is actively switched to a high value. The light intensity growths proportional to $2g_0/T_R$. When the gain is depleted, the fall time mostly depends on the cavity decay time τ_p. For short Q-switched pulses a short cavity length, high gain and a large change in the cavity Q is necessary. If the Q-switch is not fast, the pulse width may be limited by the speed of the switch. Typical electro-optical and acousto-optical switches are 10 ns and 50 ns, respectively

Image removed due to copyright restrictions.

Please see:

Keller, U., Ultrafast Laser Physics, Institute of Quantum Electronics, Swiss Federal Institute of Technology, ETH Hönggerberg—HPT, CH-8093 Zurich, Switzerland.

Figure 4.6: Asymmetric actively Q-switched pulse.

For example, with a diode-pumped Nd:YAG microchip laser [6] using an electro-optical switch based on $LiTaO_3$ Q-switched pulses as short as 270 ps at repetition rates of 5 kHz, peak powers of 25 kW at an average power of 34 mW, and pulse energy of 6.8 μJ have been generated (Figure 4.7).

Image removed due to copyright restrictions.

Please see:

Kafka, J. D., and T. Baer. "Mode-locked erbium-doped fiber laser with soliton pulse shaping." *Optics Letters* 14 (1989): 1269-1271.

Figure 4.7: Q-switched microchip laser using an electro-optic switch. The pulse is measured with a sampling scope [8]

Similar results were achieved with Nd:YLF [7] and the corresponding setup is shown in Fig. 4.8.

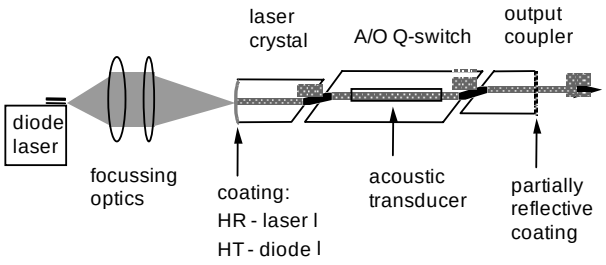

Figure 4.8: Set-up of an actively Q-switched laser.

4.4.2 Single-Frequency Q-Switched Pulses

Q-switched lasers only deliver stable output if they oscillate single frequency. Usually this is not automatically achieved. One method to achieve this is by seeding with a single-frequency laser during Q-switched operation, so that there is already a population in one of the longitudinal modes before the pulse is building up. This mode will extract all the energy before the other modes can do, see Figure 4.9

Figure 4.9: Output intenisity of a Q-switched laser without a) and with seeding b).

Another possibility to achieve single-mode output is either using an etalon in the cavity or making the cavity so short, that only one longitudinal mode is within the gain bandwidth (Figure 4.10). This is usually only the case if the cavity length is on the order of a view millimeters or below.The microchip laser [6][11][10] can be combined with an electro-optic modulator to achieve

very compact high peak power lasers with sub-nanosecond pulsewidth (Figure 4.7).

Image removed due to copyright restrictions.

Please see:
Keller, U., Ultrafast Laser Physics, Institute of Quantum Electronics, Swiss Federal Institute of Technology, ETH Hönggerberg—HPT, CH-8093 Zurich, Switzerland.

Figure 4.10: In a microchip laser the resonator can be so short, that there is only one longitudinal mode within the gain bandwidth.

4.4.3 Theory of Active Q-Switching

We want to get some insight into the pulse built-up and decay of the actively Q-switched pulse. We consider the ideal situation, where the loss of the laser cavity can be instantaneously switched from a high value to a low value, i.e. the quality factor is switched from a low value to a high value, respectively (Figure: 4.11)

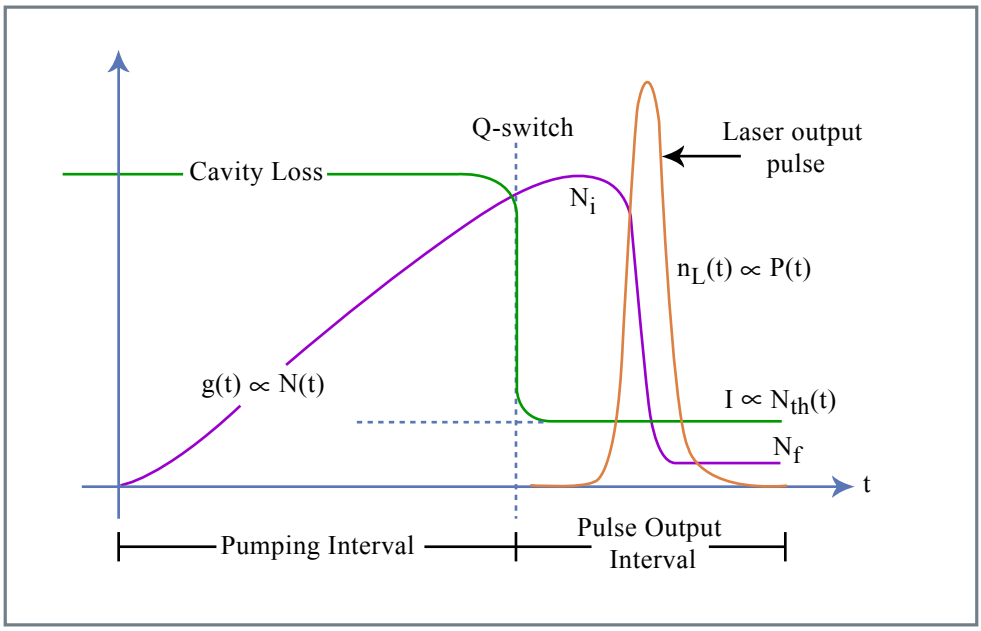

Figure 4.11: Acitve Q-Switching dynamics assuming an instantaneous switching [16].

Figure by MIT OCW.

Pumping Interval:

During pumping with a constant pump rate R_p, proportional to the small signal gain g_0, the inversion is built up. Since there is no field present, the gain follows the simple equation:

$$\frac{d}{dt}g = -\frac{g - g_0}{\tau_L}, \tag{4.33}$$

or

$$g(t) = g_0(1 - e^{-t/\tau_L}), \tag{4.34}$$

Pulse Built-up-Phase:

Assuming an instantaneous switching of the cavity losses we look for an approximate solution to the rate equations starting of with the initial gain or inversion $g_i = hf_L N_{2i}/(2E_{sat}) = hf_L N_i/(2E_{sat})$, we can savely leave the index away since there is only an upper state population. We further assume that during pulse built-up the stimulated emission rate is the dominate term changing the inversion. Then the rate equations simplify toτ

$$\frac{d}{dt}g = -\frac{gP}{E_{sat\,p}} \tag{4.35}$$

$$\frac{d}{dt}P = \frac{2(g-l)}{T_R}P, \tag{4.36}$$

resulting in

$$\frac{dP}{dg} = \frac{2E_{sat}}{T_R}\left(\frac{l}{g} - 1\right). \tag{4.37}$$

We use the following inital conditions for the intracavity power $P(t=0) = 0$ and initial gain $g(t=0) = g_i = r \cdot l$. Note, r means how many times the laser is pumped above threshold after the Q-switch is operated and the intracavity losses have been reduced to l. Then 4.37 can be directly solved and we obtain

$$P(t) = \frac{2E_{sat}}{T_R}\left(g_i - g(t) + l\ln\frac{g(t)}{g_i}\right). \tag{4.38}$$

From this equation we can deduce the maximum power of the pulse, since the growth of the intracavity power will stop when the gain is reduced to the losses, g(t)=l, (Figure 4.11)

$$P_{\max} = \frac{2lE_{sat}}{T_R}(r - 1 - \ln r) \tag{4.39}$$

$$= \frac{E_{sat}}{\tau_p}(r - 1 - \ln r). \tag{4.40}$$

This is the first important quantity of the generated pulse and is shown normalized in Figure 4.12.

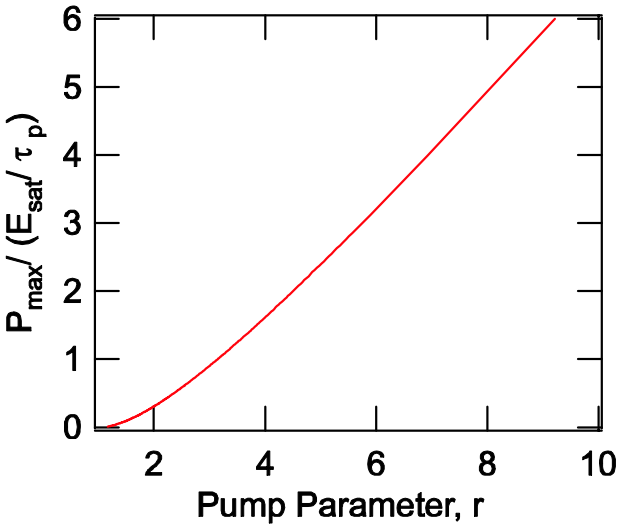

Figure 4.12: Peak power of emitted pulse as function of pump parameter.

Next, we can find the final gain g_f, that is reached once the pulse emission is completed, i.e. that is when the right side of (4.38) vanishes

$$\left(g_i - g_f + l \ln\left(\frac{g_f}{g_i}\right)\right) = 0 \tag{4.41}$$

Using the pump parameter $r = g_i/l$, this gives as an expression for the ratio between final and initial gain or between final and initial inversion

$$1 - \frac{g_f}{g_i} + \frac{1}{r} \ln\left(\frac{g_f}{g_i}\right) = 0, \tag{4.42}$$

$$1 - \frac{N_f}{N_i} + \frac{1}{r} \ln\left(\frac{N_f}{N_i}\right) = 0, \tag{4.43}$$

which depends only on the pump parameter. Assuming further, that there are no internal losses, then we can estimate the pulse energy generated by

$$E_P = (N_i - N_f)\, h f_L. \tag{4.44}$$

This is also equal to the output coupled pulse energy since no internal losses are assumed. Thus, if the final inversion gets small all the energy stored in

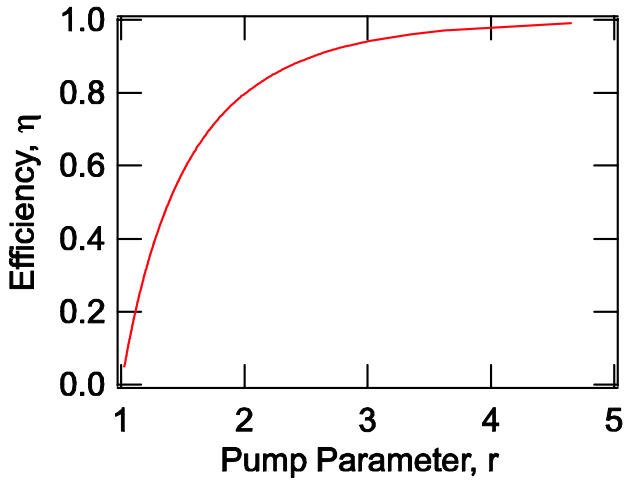

Figure 4.13: Energy extraction efficiency as a function of pump power.

the gain medium can be extracted. We define the energy extraction efficiency η

$$\eta = \frac{N_i - N_f}{N_i}, \tag{4.45}$$

that tells us how much of the initially stored energy can be extracted using eq.(4.43)

$$\eta + \frac{1}{r}\ln(1-\eta) = 0. \tag{4.46}$$

This efficiency is plotted in Figure 4.13.

Note, the energy extraction efficiency only depends on the pump parameter r. Now, the emitted pulse energy can be written as

$$E_P = \eta(r) N_i h f_L. \tag{4.47}$$

and we can estimate the pulse width of the emitted pulse by the ratio between pulse energy and peak power using (4.40) and (4.47)

$$\begin{aligned} \tau_{Pulse} &= \frac{E_P}{2lP_{peak}} = \tau_p \frac{\eta(r)}{(r-1-\ln r)} \frac{N_i h f_L}{2lE_{sat}} \\ &= \tau_p \frac{\eta(r)}{(r-1-\ln r)} \frac{g_i}{l} \\ & \tau_p \frac{\eta(r)\cdot r}{(r-1-\ln r)}. \end{aligned} \tag{4.48}$$

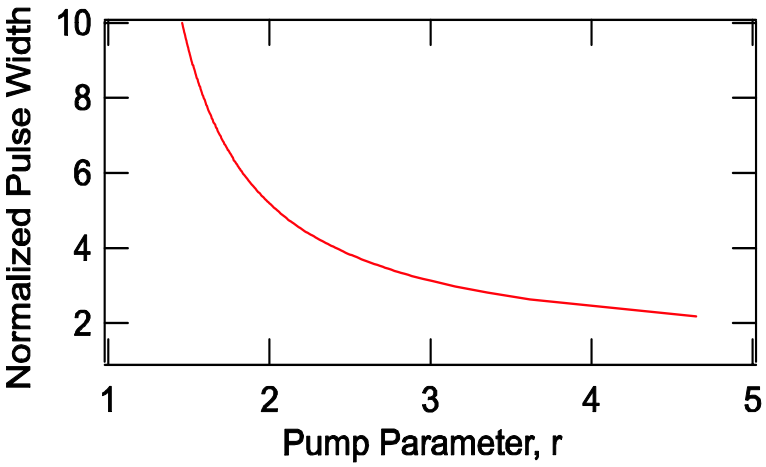

Figure 4.14: Normalized pulse width as a function of pump parameter.

The pulse width normalized to the cavity decay time τ_p is shown in Figure 4.14.

4.4.4 Passive Q-Switching

In the case of passive Q-switching the intracavity loss modulation is performed by a saturable absorber, which introduces large losses for low intensities of light and small losses for high intensity.

Relaxation oscillations are due to a periodic exchange of energy stored in the laser medium by the inversion and the light field. Without the saturable absorber these oscillations are damped. If for some reason there is two much gain in the system, the light field can build up quickly. Especially for a low gain cross section the backaction of the growing laser field on the inversion is weak and it can grow further. This growth is favored in the presence of loss that saturates with the intensity of the light. The laser becomes unstabile, the field intensity growth as long as the gain does not saturate below the net loss, see Fig.4.15.

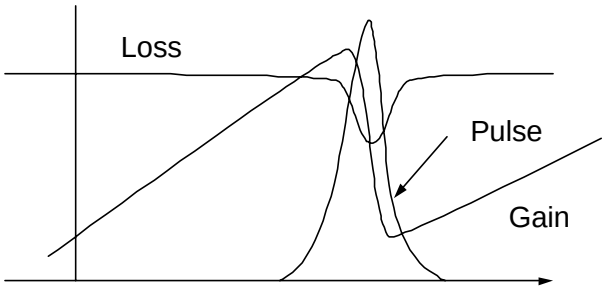

Figure 4.15: Gain and loss dynamics of a passively Q-switched laser

Now, we want to show that the saturable absorber leads to a destabilization of the relaxation oscillations resulting in the giant pulse laser.

We extend our laser model by a saturable absorber as shown in Fig. 4.16

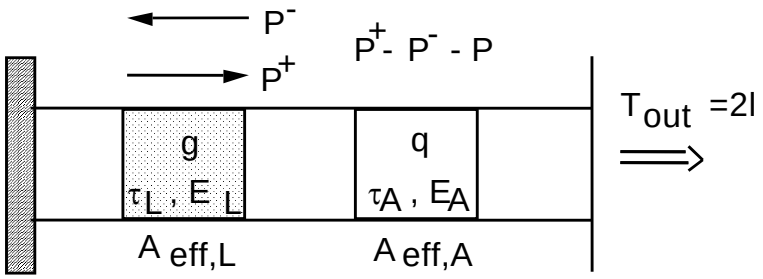

Figure 4.16: Simple laser model described by rate equations. We assume small output coupling so that the laser power within one roundtrip can be considered position independent. Neglecting standing wave effects in the cavity, the field density is related to twice the circulating power P^+ or P^-.

Rate equations for a passively Q-switched laser

We make the following assumptions: First, the transverse relaxation times of the equivalent two level models for the laser gain medium and for the saturable absorber are much faster than any other dynamics in our system, so that we can use rate equations to describe the laser dynamics. Second, we assume that the changes in the laser intensity, gain and saturable absorption

are small on a time scale on the order of the round-trip time T_R in the cavity, (i.e. less than 20%). Then, we can use the rate equations of the laser as derived above plus a corresponding equation for the saturable loss q similar to the equation for the gain.

$$T_R \frac{dP}{dt} = 2(g - l - q)P \tag{4.49}$$

$$T_R \frac{dg}{dt} = -\frac{g - g_0}{T_L} - \frac{gT_R P}{E_L} \tag{4.50}$$

$$T_R \frac{dq}{dt} = -\frac{q - q_0}{T_A} - \frac{qT_R P}{E_A} \tag{4.51}$$

where P denotes the laser power, g the amplitude gain per roundtrip, l the linear amplitude losses per roundtrip, g_0 the small signal gain per roundtrip and q_0 the unsaturated but saturable losses per roundtrip. The quantities $T_L = \tau_L/T_R$ and $T_A = \tau_A/T_R$ are the normalized upper-state lifetime of the gain medium and the absorber recovery time, normalized to the round-trip time of the cavity. The energies $E_L = h\nu A_{eff,L}/2^*\sigma_L$ and $E_A = h\nu A_{eff,A}/2^*\sigma_A$ are the saturation energies of the gain and the absorber, respectively. .

For solid state lasers with gain relaxation times on the order of $\tau_L \approx 100$ μs or more, and cavity round-trip times $T_R \approx 10$ ns, we obtain $T_L \approx 10^4$. Furthermore, we assume absorbers with recovery times much shorter than the round-trip time of the cavity, i.e. $\tau_A \approx 1 - 100$ ps, so that typically $T_A \approx 10^{-4}$ to 10^{-2}. This is achievable in semiconductors and can be engineered at will by low temperature growth of the semiconductor material [20, 30]. As long as the laser is running cw and single mode, the absorber will follow the instantaneous laser power. Then, the saturable absorption can be adiabatically eliminated, by using eq.(4.51)

$$q = \frac{q_0}{1 + P/P_A} \quad \text{with} \quad P_A = \frac{E_A}{\tau_A}, \tag{4.52}$$

and back substitution into eq.(4.49). Here, P_A is the saturation power of the absorber. At a certain amount of saturable absorption, the relaxation oscillations become unstable and Q-switching occurs. To find the stability criterion, we linearize the system

$$T_R \frac{dP}{dt} = (g - l - q(P))P \tag{4.53}$$

$$T_R \frac{dg}{dt} = -\frac{g - g_0}{T_L} - \frac{gT_R P}{E_L}. \tag{4.54}$$

Stationary solution

As in the case for the cw-running laser the stationary operation point of the laser is determined by the point of zero net gain

$$\begin{aligned} g_s &= l + q_s \\ \frac{g_0}{1 + P_s/P_L} &= l + \frac{q_0}{1 + P_s/P_A}. \end{aligned} \tag{4.55}$$

The graphical solution of this equation is shown in Fig. 4.17

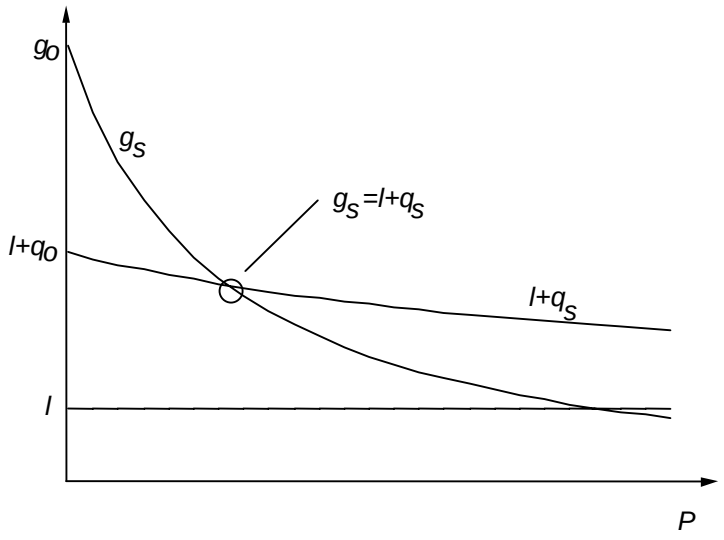

Figure 4.17: Graphical solution of the stationary operating point.

Stability of stationary operating point or the condition for Q-switching

For the linearized system, the coefficient matrix corresponding to Eq.(4.25) changes only by the saturable absorber [23]:

$$T_R \frac{d}{dt} \begin{pmatrix} \Delta P_0 \\ \Delta g_0 \end{pmatrix} = A \begin{pmatrix} \Delta P_0 \\ \Delta g_0 \end{pmatrix}, \text{ with } A = \begin{pmatrix} -2 \left.\frac{dq}{dP}\right|_{cw} P_s & 2P_s \\ -\frac{g_s T_R}{E_L} & -\frac{T_R}{\tau_{stim}} \end{pmatrix} \tag{4.56}$$

The coefficient matrix A does have eigenvalues with negative real part, if and only if its trace is negative and the determinante is positive which results in

two conditions

$$-2P\frac{dq}{dP}\bigg|_{cw} < \frac{r}{T_L} \quad \text{with} \quad r = 1 + \frac{P_A}{P_L} \quad \text{and} \quad P_L = \frac{E_L}{\tau_L}, \tag{4.57}$$

and

$$\frac{dq}{dP}\bigg|_{cw} \frac{r}{T_L} + 2g_s\frac{r-1}{T_L} > 0. \tag{4.58}$$

After cancelation of T_L we end up with

$$\left|\frac{dq}{dP}\bigg|_{cw}\right| < \left|\frac{dg_s}{dP}\bigg|_{cw}\right|. \tag{4.59}$$

For a laser which starts oscillating on its own, relation 4.59 is automatically fulfilled since the small signal gain is larger than the total losses, see Fig. 4.17. Inequality (4.57) has a simple physical explanation. The right hand side of (4.57) is the relaxation time of the gain towards equilibrium, at a given pump power and constant laser power. The left hand side is the decay time of a power fluctuation of the laser at fixed gain. If the gain can not react fast enough to fluctuations of the laser power, relaxation oscillations grow and result in passive Q-switching of the laser.

As can be seen from Eq.(4.55) and Eq.(4.57), we obtain

$$-2T_L P\frac{dq}{dP}\bigg|_{cw} = 2T_L q_0 \frac{\frac{P}{\chi P_L}}{\left(1+\frac{P}{\chi P_L}\right)^2}\bigg|_{cw} < r_s \quad \text{with} \quad \chi = \frac{P_A}{P_L}, \tag{4.60}$$

where χ is an effective "stiffness" of the absorber against cw saturation. The stability relation (4.60) is visualized in Fig. 4.18.

Figure 4.18: Graphical representation of cw-Q-switching stability relation for different products $2q_0T_L$. The cw-stiffness used for the the plots is $\chi = 100$.

The tendency for a laser to Q-switch increases with the product q_0T_L and decreases if the saturable absorber is hard to saturate, i.e. $\chi \gg 1$. As can be inferred from Fig. 4.18 and eq.(4.60), the laser can never Q-switch, i.e. the left side of eq.(4.60) is always smaller than the right side, if the quantity

$$MDF = \frac{2q_0T_L}{\chi} < 1 \tag{4.61}$$

is less than 1. The abbreviation MDF stands for mode locking driving force, despite the fact that the expression (4.61) governs the Q-switching instability. We will see, in the next section, the connection of this parameter with mode locking. For solid-state lasers with long upper state life times, already very small amounts of saturable absorption, even a fraction of a percent, may lead to a large enough mode locking driving force to drive the laser into Q-switching. Figure 4.19 shows the regions in the $\chi - P/P_L$ - plane where Q-switching can occur for fixed MDF according to relation (4.60). The area above the corresponding MDF-value is the Q-switching region. For MDF $<$ 1, cw-Q-switching can not occur. Thus, if a cw-Q-switched laser has to be designed, one has to choose an absorber with a MDF $>$1. The further the operation point is located in the cw-Q-switching domain the more pronounced the cw-Q-switching will be. To understand the nature of the instability we look at the eigen solution and eigenvalues of the linearized equations of mo-

Image removed due to copyright restrictions.

Please see:
Kaertner, Franz, et al. "Control of solid state laser dynamics by semiconductor devices." *Optical Engineering* 34, no. 7 (July 1995): 2024-2036.

Figure 4.19: For a given value of the MDF, cw-Q-switching occurs in the area above the corresponding curve. For a MDF-value less than 1 cw-Qswitching can not occur.

tion 4.56

$$\frac{d}{dt}\begin{pmatrix}\Delta P_0(t)\\ \Delta g_0(t)\end{pmatrix} = s\begin{pmatrix}\Delta P_0(t)\\ \Delta g_0(t)\end{pmatrix} \tag{4.62}$$

which results in the eigenvalues

$$sT_R = \frac{A_{11}+A_{22}}{2} \pm j\sqrt{A_{11}A_{22} - A_{12}A_{21} - \left(\frac{A_{11}+A_{22}}{2}\right)^2}. \tag{4.63}$$

With the matrix elements according to eq.(4.56) we get

$$s = \frac{-\frac{2}{T_R}\left.\frac{dq}{dP}\right|_{cw} P_s - \frac{1}{\tau_{stim}}}{2} \pm j\omega_Q \tag{4.64}$$

$$\omega_Q = \sqrt{-\frac{2}{T_R}\left.\frac{dq}{dP}\right|_{cw} P_s\frac{r}{\tau_L} + \frac{r-1}{\tau_p\tau_L} - \left(\frac{-\frac{2}{T_R}\left.\frac{dq}{dP}\right|_{cw} P_s - \frac{1}{\tau_{stim}}}{2}\right)^2} \tag{4.65}$$

where the pump parameter is now defined as the ratio between small signal gain the total losses in steady state, i.e. $r = g_0/(l+q_s)$. This somewhat lengthy expression clearly shows, that when the system becomes unstable,

$-2\,\frac{dq}{dP}\big|_{cw} P_s > \frac{T_R}{\tau_{stim}}$, with $\tau_L \gg \tau_p$, there is a growing oscillation with frequency

$$\omega_Q \approx \sqrt{\frac{r-1}{\tau_p \tau_L}} \approx \sqrt{\frac{1}{\tau_p \tau_{stim}}}. \tag{4.66}$$

That is, passive Q-switching can be understood as a destabilization of the relaxation oscillations of the laser. If the system is only slightly in the instable regime, the frequency of the Q-switching oscillation is close to the relaxation oscillation frequency. If we define the growth rate γ_Q, introduced by the saturable absorber as a prameter, the eigen values can be written as

$$s = \frac{1}{2}\left(\gamma_Q - \frac{1}{\tau_{stim}}\right) \pm j\sqrt{\gamma_Q \frac{r}{\tau_L} + \frac{r-1}{\tau_p \tau_L} - \left(\frac{\gamma_Q - \frac{1}{\tau_{stim}}}{2}\right)^2}. \tag{4.67}$$

Figure 4.20 shows the root locus plot for a system with and without a saturable absorber. The saturable absorber destabilizes the relaxation oscillations. The type of bifurcation is called a Hopf bifurcation and results in an oscillation.

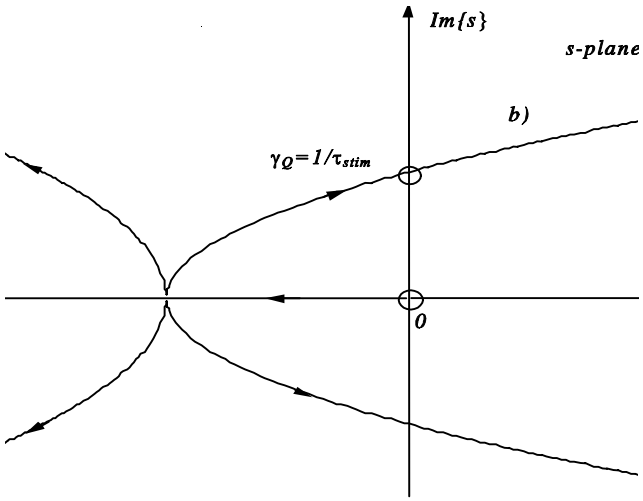

Figure 4.20: Root locus plot for the linearized rate equations. a) Without saturable absorber as a function of the pump parameter r; b) With saturable absorber as a function of γ_Q .

As an example, we consider a laser with the following parameters: $\tau_L = 250\mu s$, $T_R = 4ns$, $2l_0 = 0.1$, $2q_0 = 0.005$, $2g_0 = 2$, $P_L/P_A = 100$. The rate equations are solved numberically and shown in Figures4.21 and 4.22.

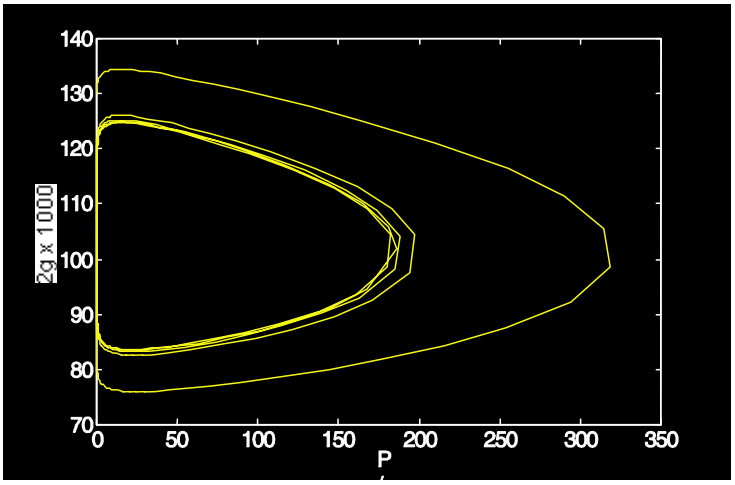

Figure 4.21: Phase space plot of the rate equations. It takes several oscillations, until the steady state limit cycle is reached.

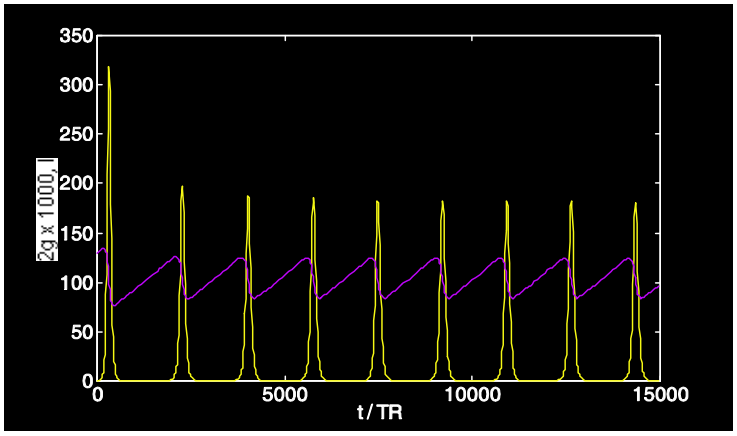

Figure 4.22: Solution for gain and output power as a function of time.

4.5 Example: Single Mode CW-Q-Switched Microchip Lasers

Q-switched microchip lasers are compact and simple solid-state lasers, which can provide a high peak power with a diffraction limited output beam. Due to the extremely short cavity length, typically less than 1 mm, single-frequency Q-switched operation with pulse widths well below a ns can be achieved. Pulse durations of 337 ps and 218 ps have been demonstrated with a passively Q-switched microchip laser consisting of a Nd:YAG crystal bonded to a thin piece of Cr^{4+}:YAG [8, 9]. Semiconductor saturable absorbers were used to passively Q-switch a monolithic Nd:YAG laser producing 100 ns pulses [38].

4.5.1 Set-up of the Passively Q-Switched Microchip Laser

Figure 4.23(a) shows the experimental set-up of the passively Q-switched microchip laser and Fig. 4.23(b) the structure of the semiconductor saturable absorber [12, 13]. The saturable absorber structure is a so called anti-resonant Fabry-Perot saturable absorber (A-FPSA), because in a microchip laser the beam size is fixed by the thermal lens that builds up in the laser crystal, when pumped with the diode laser. Thus, one can use the top reflector of the A-FPSA to scale the effective saturation intensity of the absorber with respect to the intracavity power. The 200 or 220 μm thick Nd:YVO_4 or Nd:LaSc3(BO3)4, (Nd:LSB) laser crystal [39] is sandwiched between a 10% output coupler and the A-FPSA. The latter is coated for high reflection at the pump wavelength of 808 nm and a predesigned reflectivity at the laser wavelength of 1.062 μ m, respectively. The laser crystals are pumped by a semiconductor diode laser at 808 nm through a dichroic beamsplitter, that transmits the pump light and reflects the output beam at 1.064 μm for the Nd:YVO_4 or 1.062 μm for the Nd:LSB laser. To obtain short Q-switched pulses, the cavity has to be as short as possible. The highly doped laser crystals with a short absorption length of only about $100\mu m$ lead to a short but still efficient microchip laser [13]. The saturable absorber consists of a dielectric top mirror and 18 pairs of GaAs/InGaAs MQW's grown on a GaAs/AlAs Bragg-mirror. The total optical thickness of the absorber is on the order of 1 μm. Therefore, the increase of the cavity length due to the

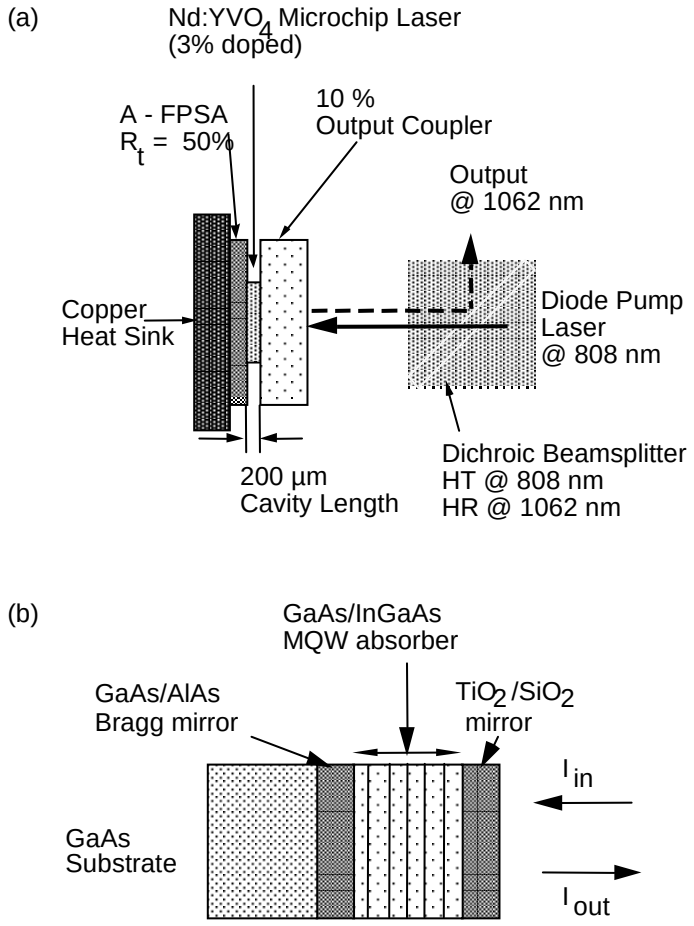

Figure 4.23: /a) Experimental set-up of the cw-passively Q-switched Nd:YVO_4 microchip-laser. (b) Structure of the anti-resonant Fabry-Perot semiconductor saturable absorber [37].

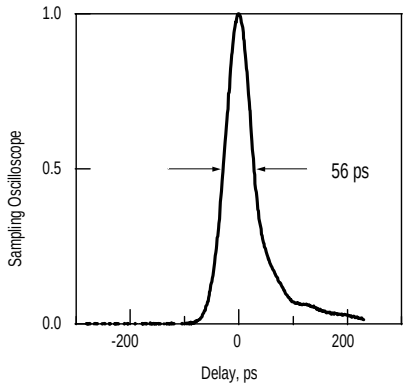

Figure 4.24: Single-Mode Q-switched pulse achieved with Nd:YVO_4 microchip laser.

absorber is neglegible. For more details see [12, 13]. Pulses as short as 56 ps, Fig. (4.24), have been achieved with Nd:LSB-crystals.

4.5.2 Dynamics of a Q-Switched Microchip Laser

The passively Q-switched microchip laser, shown in Fig. 4.23(a), is perfectly modelled by the rate equations (4.49) to (4.51). To understand the basic dependence of the cw-Q-switching dynamics on the absorber parameters, we performed numerical simulations of the Nd:LSB microchip laser, as shown in Fig. 4.23. The parameter set used, is given in Table 4.2. For these parameters, we obtain according to eq.(4.55) a mode locking driving force of $MDF = 685$. This laser operates clearly in the cw-Q-switching regime as soon as the laser is pumped above threshold. Note, the Q-switching condition (4.61) has only limited validity for the microchip laser considered here, because, the cavity length is much shorter than the absorber recovery time. Thus the adiabatic elimination of the absorber dynamics is actually not any longer justified. Figures 4.25 and 4.26 show the numerical solution of the set of rate equations (4.49) to (4.51) on a microsecond timescale and a picosecond timescale close to one of the pulse emission events.

No analytic solution to the set of rate equations is known. Therefore, optimization of Q-switched lasers has a long history [4, 5], which in general results in complex design criteria [5], if the most general solution to the rate

parameter	value
$2\ g_0$	0.7
$2\ q_0$	0.03
$2\ l$	0.14
T_R	2.7 ps
τ_L	87 μs
τ_A	24 ps
E_L	20 μJ
E_A	7.7 nJ

Table 4.2: Parameter set used for the simulation of the dynamics of the Q-switched microchip laser.

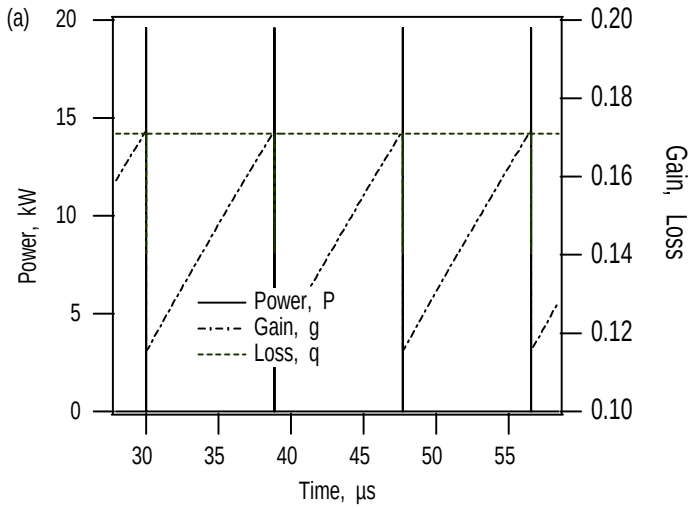

Figure 4.25: Dynamics of the Q-switched microchip laser by numerical solution of the rate equatioins on a microsecond timescale.

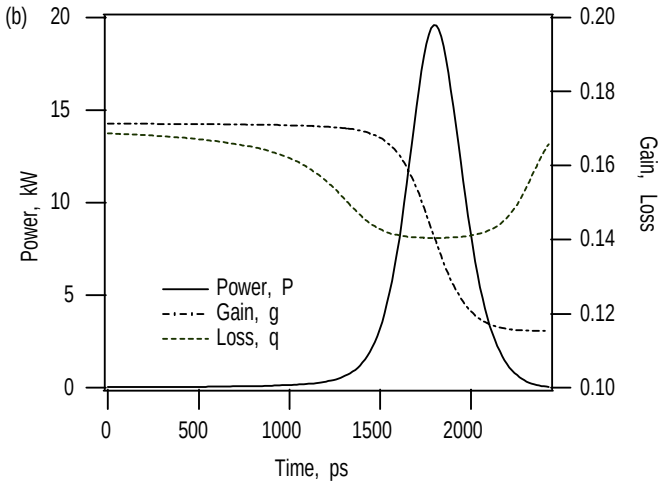

Figure 4.26: Dynamics of the Q-switched microchip laser by numerical solution of the rate equatioins on a picosecond timescale.

equations is considered. However, a careful look at the simulation results leads to a set of very simple design criteria, as we show in the following. As seen from Fig. 4.25, the pulse repetition time T_{rep} is many orders of magnitude longer than the width of a Q-switched pulse. Thus, between two pulse emissions, the gain increases due to pumping until the laser reaches threshold. This is described by eq.(4.50), where the stimulated emission term can be neglected. Therfore, the pulse repetition rate is determined by the relation that the gain has to be pumped to threshold again $g_{th} = l + q_0$, if it is saturated to the value g_f after pulse emission. In good approximation, $g_f = l - q_0$, as long as it is a positive quantity. If $T_{rep} < \tau_L$, one can linearize the exponential and we obtain

$$g_{th} - g_f = g_0 \frac{T_{rep}}{\tau_L} \tag{4.68}$$

$$T_{rep} = \tau_L \frac{g_{th} - g_f}{g_0} = \tau_L \frac{2q_0}{g_0}. \tag{4.69}$$

Figure 4.26 shows, that the power increases, because, the absorber saturates faster than the gain. To obtain a fast raise of the pulse, we assume an absorber which saturates much easier than the gain, i.e. $E_A \ll E_L$, and the

recovery times of gain and absorption shall be much longer than the pulse width τ_{pulse}, $\tau_A \gg \tau_{pulse}$. Since, we assume a slow gain and a slow absorber, we can neglect the relaxation terms in eqs.(4.50) and (4.51) during growth and decay of the pulse. Then the equations for gain and loss as a function of the unknown Q-switched pulse shape $f_Q(t)$

$$P(t) = E_P f_Q(t) \tag{4.70}$$

can be solved. The pulse shape $f_Q(t)$ is again normalized, such that its integral over time is one and E_P is, therefore, the pulse energy. Analogous to the derivation for the Q-switched mode locking threshold in eqs.(4.84) and (4.85), we obtain

$$q(t) = q_0 \exp\left[-\frac{E_P}{E_A}\int_{-\infty}^{t} f_Q(t')dt'\right], \tag{4.71}$$

$$g(t) = g_{th} \exp\left[-\frac{E_P}{E_L}\int_{-\infty}^{t} f_Q(t')dt'\right]. \tag{4.72}$$

Substitution of these expressions into the eq.(4.49) for the laser power, and integration over the pulse width, determines the extracted pulse energy. The result is a balance between the total losses and the gain.

$$l + q_P(E_P) = g_P(E_P) \tag{4.73}$$

with

$$q_P(E_P) = q_0 \frac{1 - \exp\left[-\frac{E_P}{E_A}\right]}{\frac{E_P}{E_A}}, \tag{4.74}$$

$$g_P(E_P) = g_{th} \frac{1 - \exp\left[-\frac{E_P}{E_L}\right]}{\frac{E_P}{E_L}}. \tag{4.75}$$

Because, we assumed that the absorber is completely saturated, we can set $q_P(E_P) \approx 0$. Figure 4.27 shows the solution of eq.(4.73), which is the pulse energy as a function of the ratio between saturable and nonsaturable losses $s = q_0/l$. Also approximate solutions for small and large s are shown as the dashed curves. Thus, the larger the ratio between saturable and nonsaturable losses is, the larger is the intracavity pulse energy, which is not

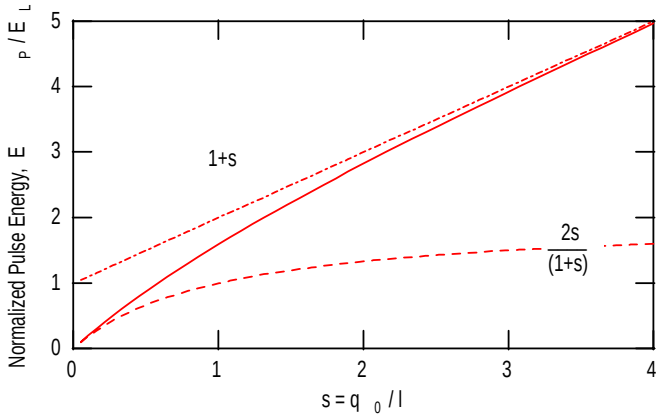

Figure 4.27: (—) Intracavity pulse energy as a function of the ratio between saturable and nonsaturable losses s. (- - -) Approximations for small and large values for s.

surprising. Note, the extracted pulse energy is proportional to the output coupling, which is $2l$ if no other losses are present. If we assume, $s << 1$, then, we can use approximately the low energy approximation

$$E_P = 2E_L \frac{q_0}{l + q_0}. \tag{4.76}$$

The externally emitted pulse energy is then given by

$$E_P^{ex} = 2lE_P = E_L \frac{4lq_0}{l + q_0}. \tag{4.77}$$

Thus, the total extracted pulse energy is completely symmetric in the saturable and non saturable losses. For a given amount of saturable absorption, the extracted pulse energy is maximum for an output coupling as large as possible. Of course threshold must still be reached, i.e. $l + q_0 < g_0$. Thus, in the following, we assume $l > q_0$ as in Fig. 4.26. The absorber is immediatelly bleached, after the laser reaches threshold. The light field growth and extracts some energy stored in the gain medium, until the gain is saturated to the low loss value l. Then the light field decays again, because the gain is below the loss. During decay the field can saturate the gain by a similar amount as during build-up, as long as the saturable losses are smaller than

the constant output coupler losses l, which we shall assume in the following. Then the pulse shape is almost symmetric as can be seen from Fig. 4.26(b) and is well approximated by a secant hyperbolicus square for reasons that will become obvious in a moment. Thus, we assume

$$f_Q(t) = \frac{1}{2\tau_P}\mathrm{sech}^2\left(\frac{t}{\tau_p}\right). \tag{4.78}$$

With the assumption of an explicite pulse form, we can compute the pulse width by substitution of this ansatz into eq.(4.49) and using (4.71), (4.72)

$$-\frac{2T_R}{\tau_P}\tanh\left(\frac{t}{\tau_p}\right) = g_{th}\exp\left[-\frac{E_P}{2E_L}\left(1+\tanh\left(\frac{t}{\tau_p}\right)\right)\right] - l. \tag{4.79}$$

Again, we neglect the saturated absorption. If we expand this equation up to first order in E_P/E_L and compare coefficients, we find from the constant term the energy (4.77), and from the tanh-term we obtain the following simple expression for the pulse width

$$\tau_P = 2\frac{T_R}{q_0}. \tag{4.80}$$

For the FWHM pulse width of the resulting sech^2-pulse we obtain

$$\tau_{P,FWHM} = 3.5\frac{T_R}{q_0}. \tag{4.81}$$

Thus, for optimium operation of a Q-switched microchip laser, with respect to minimum pulse width and maximum extracted energy in the limits considered here, we obtain a very simple design criterium. If we have a maximum small signal round-trip gain g_0, we should design an absorber with q_0 somewhat smaller than $g_0/2$ and an output coupler with $q_0 < l < g_0 - q_0$, so that the laser still fullfills the cw-Q-switching condition. It is this simple optimization, that allowed us to reach the shortest pulses every generated from a cw-Q-switched solid-state laser. Note, for a maximum saturable absorption of 2 $q_0 = 13\%$, a cavity roundtip time of $T_R = 2.6$ ps for the Nd:YVO_4 laser, one expects from (4.81) a pulse width of about $\tau_P = 70ps$, which is close to what we observed in the experiment above. We achieved pulses between 56 and 90 ps [13]. The typical extracted pulse energies were on the order of E_P = 0.1 - 0.2 μJ for pulses of about $60ps$ [13]. Using a saturation energy of

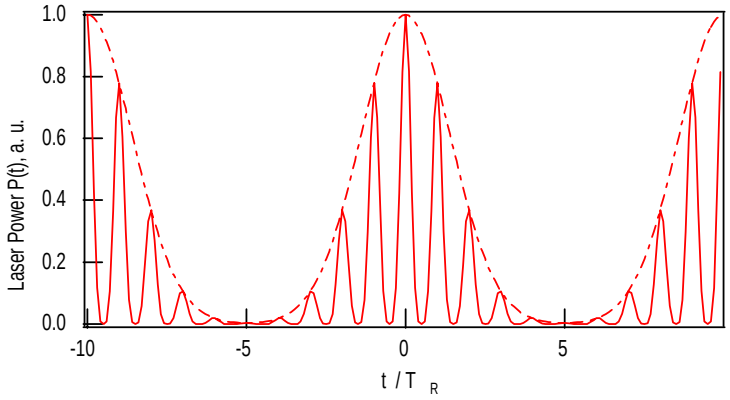

Figure 4.28: Laser output power as a function of time, when operating in the Q-switched mode-locked regime.

about $E_L = 30\ \mu$J and an output coupler loss of $2l = 0.1$, we expect, according to (4.77), a maximum extracted pulse energy of $E_P^{ex} = 2\ \mu$J. Thus, we have a deviation of one order of magnitude, which clearly indicates that the absorber still introduces too much of nonsaturable intracavity losses. Lowering of these losses should lead to μJ - 50 ps pulses from this type of a very simple and cheap laser, when compared with any other pulse generation technique.

4.6 Q-Switched Mode Locking

To understand the regime of Q-switched mode locking, we reconsider the rate equations (4.49) to (4.51). Fig. 4.28 shows, that we can describe the laser power on two time scales. One is on the order of the Q-switching envelope and occurs on multiple round-trips in the laser cavity, $T = mT_R$. Therefore, it is on the order of microseconds. The other time scale t is a short time scale on the order of the pulse width, i.e. picoseconds. Assuming a normalized pulse shape $f_n(t)$ for the n-th pulse such that

$$\int_{-T_R/2}^{T_R/2} f_n(t - nT_R)dt = 1, \tag{4.82}$$

we can make the following ansatz for the laser power

$$P(T,t) = E_P(T) \sum_{n=-\infty}^{\infty} f_n(t - nT_R). \tag{4.83}$$

Here, $E_P(T = mT_R)$ is the pulse energy of the m-th pulse, which only changes appreciably over many round-trips in the cavity. The shape of the m-th pulse, $f_m(t)$, is not yet of further interest. For simplicity, we assume that the mode-locked pulses are much shorter than the recovery time of the absorber. In this case, the relaxation term of the absorber in Eq.(4.52) can be neglected during the duration of the mode-locked pulses. Since the absorber recovery time is assumed to be much shorter than the cavity round-trip time, the absorber is unsaturated before the arrival of a pulse. Thus, for the saturation of the absorber during one pulse, we obtain

$$q(T = mT_R, t) = q_0 \exp\left[-\frac{E_P(T)}{E_A} \int_{-T_R/2}^{t} f_m(t')dt'\right]. \tag{4.84}$$

Then, the loss in pulse energy per roundtrip can be written as

$$q_P(T) = \int_{-T_R/2}^{T_R/2} f_m(t) q(T = mT_R, t)dt = q_0 \frac{1 - \exp\left[-\frac{E_P(T)}{E_A}\right]}{\frac{E_P(T)}{E_A}}. \tag{4.85}$$

Eq. (4.85) shows that the saturable absorber saturates with the pulse energy and not with the average intensity of the laser, as in the case of cw-Q-switching (4.52). Therefore, the absorber is much more strongly bleached at the same average power. After averaging Eqs.(4.49) and (4.50) over one round-trip, we obtain the following two equations for the dynamics of the pulse energy and the gain on a coarse grained time scale T:

$$T_R \frac{dE_P}{dT} = 2(g - l - q_P(E_P))E_P, \tag{4.86}$$

$$T_R \frac{dg}{dT} = -\frac{g - g_0}{T_L} - \frac{gE_P}{E_L}. \tag{4.87}$$

This averaging is allowed, because the saturation of the gain medium within one pulse is negligible, due to the small interaction cross section of the solid-state laser material. Comparing Eqs.(4.49), (4.50) and (4.52) with (4.84), (4.86) and (4.87), it becomes obvious that the stability criterion (4.53)

also applies to Q-switched mode locking if we replace the formula for cw-saturation of the absorber (4.52) by the formula for pulsed saturation (4.85). Then, stability against Q-switched mode locking requires

$$-2E_P \frac{dq_P}{dE_P}\bigg|_{cw-mod} < \frac{r}{T_L}\bigg|_{cw-mod}, \tag{4.88}$$

with

$$-2E_P \frac{dq_P}{dE_P}\bigg|_{cw-mod} = 2q_0 \frac{1-\exp\left[-\frac{E_P}{E_A}\right]\left(1+\frac{E_P}{E_A}\right)}{\frac{E_P}{E_A}}. \tag{4.89}$$

When expressed in terms of the average power $P = E_P/T_R$, similar to Eq.(4.60), we obtain

$$-2T_L E_P \frac{dq_P}{dE_P}\bigg|_{cw-mod} = 2T_L q_0 \frac{1-\exp\left[-\frac{P}{\chi_P P_L}\right]\left(1+\frac{P}{\chi_P P_L}\right)}{\frac{P}{\chi_P P_L}}, \tag{4.90}$$

where $\chi_P = \chi T_A$ describes an effective stiffness of the absorber compared with the gain when the laser is cw-mode-locked at the same average power as the cw laser. Thus, similar to the case of cw-Q-switching and mode locking it is useful to introduce the driving force for Q-switched mode locking

$$QMDF = \frac{2q_0 T_L}{\chi_P}. \tag{4.91}$$

Figure 4.29 shows the relation (4.88) for different absorber strength. In going from Fig. 4.18 to Fig. 4.29, we used $T_A = 0.1$. We see, that the short normalized recovery time essentially leads to a scaling of the abscissa, when going from Fig. 4.18 to Fig. 4.29 while keeping all other parameters constant. Comparing Eqs.(4.61) with (4.91), it follows that, in the case of cw-mode locking, the absorber is more strongly saturated by a factor of $1/T_A$, which can easily be as large as 1000. Therefore, the Q-switched mode locking driving force is much larger than the mode locking driving force, MDF, Accordingly, the tendency for Q-switched mode locking is significantly higher than for cw Q-switching. However, now, it is much easier to saturate the absorber with an average power well below the damage threshold of the absorber (Fig. 4.29). Therefore, one is able to leave the regime of Q-switched mode locking at a large enough intracavity power.

Image removed due to copyright restrictions.

Please see:
Kaertner, Franz, et al. "Control of solid state laser dynamics by semiconductor devices." *Optical Engineering* 34, no. 7 (July 1995): 2024-2036.

Figure 4.29: Visualization of the stability relations for Q-switched mode locking for different products $2q_0T_L$. The assumed stiffness for pulsed operation is $\chi_P = 10$, which corresponds to $T_A = 0.1$. The functional form of the relations for cw Q-switching and Q-switched mode locking is very similar. The change in the stiffness, when going from cw to pulsed saturation, thus essentially rescales the x-axis. For low-temperature grown absorbers, T_A can be as small as 10^{-6}

Image removed due to copyright restrictions.

Please see:
Kaertner, Franz, et al. "Control of solid state laser dynamics by semiconductor devices." *Optical Engineering* 34, no. 7 (July 1995): 2024-2036.

Figure 4.30: Self-Starting of mode locking and stability against Q-switched mode locking

We summarize our results for Q-switched mode locking in Fig. 4.30. It shows the stability boundary for Q-switched mode locking according to eq.(4.88), for different strengths of the saturable absorber, i.e. different values $2q_0T_L$. One may also derive minimum critical mode locking driving force for self-starting modelocking of the laser MDF_c due to various processes in the laser [24][25][27][28]. Or, with the definition of the pulsed stiffness, we obtain

$$\chi_{p,c} \leq \frac{2q_0T_L}{MDF_c}T_A. \tag{4.92}$$

Thus, for a self-starting laser which shows pure cw-mode locking, we have to design the absorber such that its MDF is greater than this critical value. Or expressed differently, the pulsed stiffness has to be smaller than the critical value $\chi_{p,c}$, at a fixed value for the absorber strength q_0. There is always a trade-off: On one hand, the mode locking driving force has to be large enough for self-starting. On the other hand the saturable absorption has to be small enough, so that the laser can be operated in a parameter regime where it is stable against Q-switching mode locking, see Fig. (4.30).

4.7 Summary

Starting from a simple two level laser and absorber model, we characterized the dynamics of solid-state lasers mode-locked and Q-switched by a saturable absorber. The unique properties of solid-state laser materials, i.e. their long upper-state life time and their small cross sections for stimulated emission, allow for a separation of the laser dynamics on at least two time scales. One process is the energy build-up and decay, which occurs typically on a time scale of the upper state lifetime or cavity decay time of the laser. The other process is the pulse shaping, which occurs within several roundtrips in the cavity. Separating these processes, we can distinguish between the different laser dynamics called cw-Q-switching, Q-switched mode locking and cw-mode locking. We found the stability boundaries of the different regimes, which give us guidelines for the design of absorbers for a given solid state laser to favour one of these regimes. Semiconductor absorbers are a good choice for saturable absorbers to modelock lasers, since the carrier lifetime can be engineered by low temperature growth [20]. When the pulses become short enough, the laser pulse saturates the absorber much more efficiently, which stabilizes the laser against undesired Q-switched mode locking. It has

been demonstrated experimentally, that this technique can control the laser dynamics of a large variety of solid-state lasers, such as Nd:YAG, Nd:YLF, Nd:$YV0_4$, [18] in the picosecond regime.

With semiconductor devices and soliton formation due to negative GVD and SPM, we can use similar semiconductor absorbers to modelock the lasers in the femtosecond regime [35]. The stability criteria derived here can be applied to both picosecond and femtosecond lasers. However, the characteristics of the absorber dynamics may change drastically when going from picosecond to femtosecond pulses [36]. Especially, the saturation energy may depend not only on excitation wavelength, but also on the pulsewidth. In addition there may be additional loss mechanismes for the pulse, for example due to soliton formation there are additional filter losses of the pulse which couple to the energy of the pulse via the area theorem. This has to be taken into account, before applying the theory to fs-laser systems, which will be discussed in more detail later.

Bibliography

[1] R. W. Hellwarth, Eds., Advances in Quantum Electronics, Columbia Press, New York (1961).

[2] A. E. Siegman, "Lasers," University Science Books, Mill Valley, California (1986).

[3] O. Svelto, "Principles of Lasers," Plenum Press, NY 1998.

[4] W. G. Wagner and B. A. Lengyel "Evolution of the Giant Pulse in a Laser," J. Appl. Opt. **34**, 2040 – 2046 (1963).

[5] J. J. Degnan, "Theory of the Optimally Coupled Q-switched Laser," IEEE J. Quantum Electron. **QE-25**, 214 – 220 (1989). and "Optimization of Passively Q-switched Lasers," IEEE J. Quantum Electron. **QE-31**, 1890 – 1901 (1995).

[6] J. J. Zayhowski, C. D. III, Optics Lett. 17, 1201 (1992)

[7] 5. H. Plaessmann, K. S. Yamada, C. E. Rich, W. M. Grossman, Applied Optics 32, 6618 (1993)

[8] J. J. Zayhowski, C. Dill, "Diode-pumped passively Q-switched picosecond microchip lasers," Opt. Lett. **19**, pp. 1427 – 1429 (1994).

[9] J. J. Zayhowski, J. Ochoa, C. Dill, "UV generation with passively Q-switched picosecond microchip lasers," Conference on Lasers and Electro Optics, (Baltimore, USA) 1995, paper CTuM2 p. 139.

[10] P. Wang, S.-H. Zhou, K. K. Lee, Y. C. Chen, "Picosecond laser pulse generation in a monolithic self-Q-switched solid-state laser," Opt. Com **114**, pp. 439 – 441 (1995).

[11] J. J. Zayhowski, "Limits imposed by spatial hole burning on the single-mode operation of standing-wave laser cavities," Opt. Lett. **15**, 431 – 433 (1990).

[12] B. Braun, F. X. Kärtner, U. Keller, J.-P. Meyn and G. Huber, "Passively Q-switched 180 ps Nd:$LaSc_3(BO_3)_4$ microchip laser," Opt. Lett. **21**, pp. 405 – 407 (1996).

[13] B. Braun, F. X. Kärtner, G. Zhang, M. Moser and U. Keller, "56 ps Passively Q-switched diode-pumped microchip laser," Opt. Lett. **22**, 381-383, 1997.

[14] O. Forster, "Analysis I, Differential- und Integralrechnung einer Veränderlichen," Vieweg, Braunschweig (1983).

[15] E. P. Ippen, "Principles of passive mode locking," Appl. Phys. **B 58**, pp. 159 – 170 (1994).

[16] A. Penzkofer, "Passive Q-switching and mode-locking for the generation of nanosecond to femtosecond Pulses," Appl. Phys. **B 46**, pp. 43 – 60 (1988).

[17] U. Keller, D. A. B. Miller, G. D. Boyd, T. H. Chiu, J. F. Ferguson, M. T. Asom, "Solid-state low-loss intracavity saturable absorber for Nd:YLF lasers: an antiresonant semiconductor Fabry-Perot saturable absorber," Opt. Lett. **17**, pp. 505 – 507 (1992).

[18] U. Keller, "Ultrafast all-solid-state laser technology," Appl. Phys. **B 58**, pp. 347-363 (1994).

[19] J. P. Meyn, "Neodym-Lanthan-Scandium-Borat: Ein neues Material für miniaturisierte Festkörperlaser," PhD Thesis, Universität Hamburg.

[20] G. L. Witt, R. Calawa, U. Mishra, E. Weber, Eds., "Low Temperature (LT) GaAs and Related Materials," **241** Pittsburgh, (1992).

[21] H. Haken, "Synergetics: An Introduction," Springer Verlag, Berlin (1983).

[22] A. Yariv, "Quantum Electronics", Wiley Interscience (1975).

[23] H. A. Haus, "Parameter ranges for cw passive modelocking," IEEE J. Quantum Electron., QE-**12**, pp. 169 – 176 (1976).

[24] E. P. Ippen, L. Y. Liu, H. A. Haus, "Self-starting condition for additive-pulse modelocked lasers," Opt. Lett. **15**, pp. 183 – 18 (1990).

[25] F. Krausz, T. Brabec, C. Spielmann, "Self-starting passive modelocking," Opt. Lett. **16**, pp. 235 – 237 (1991).

[26] H. A. Haus, E. P. Ippen, "Self-starting of passively mode-locked lasers," Opt. Lett. **16**, pp. 1331 – 1333 (1991).

[27] J. Herrmann, "Starting dynamic, self-starting condition and modelocking threshold in passive, coupled-cavity or Kerr-lens mode-locked solid-state lasers," Opt. Com. **98**, pp. 111 – 116 (1993).

[28] C. J. Chen, P. K. A. Wai and C. R. Menyuk, "Self-starting of passively modelocked lasers with fast saturable absorbers," Opt. Lett. **20**, pp. 350 – 352 (1995).

[29] R. W. Boyd, "Nonlinear Optics," Academic Press, New York, (1992).

[30] L. R. Brovelli, U. Keller, T. H. Chiu, "Design and Operation of Antiresonant Fabry-Perot Saturable Semiconductor Absorbers for Mode-Locked Solid-State Lasers," J. Opt. Soc. of Am. B **12**, pp. 311 – 322 (1995).

[31] K. Smith, E. J. Greer, R. Wyatt, P. Wheatley, N. J. Doran, "Totally integrated erbium fiber soliton laser pumped by laser diode," Electr. Lett. **27**, pp. 244 – 245 (1990).

[32] U. Keller, T. K. Woodward, D. L. Sivco, A. Y. Cho, "Coupled-Cavity Resonant Passive Modelocked Nd:Yttrium Lithium Fluoride Laser," Opt. Lett. **16** pp. 390 – 392 (1991).

[33] U. Keller, T. H. Chiu, "Resonant passive modelocked Nd:YLF laser," IEEE J. Quantum Electron. **QE-28**, pp. 1710 – 1721 (1992).

[34] G. P. Agrawal, N. A. Olsson, "Self-Phase Modulation and Spectral Broadening of Optical Pulses in Semiconductor Laser Amplifiers," IEEE J. Quantum Electron. **25**, pp. 2297 - 2306 (1989).

[35] D. Kopf, K. J. Weingarten, L. Brovelli, M. Kamp, U. Keller, "Diode-pumped 100-fs passively mode-locked Cr:LiSAF using an A-FPSA," Opt. Lett. **19**, pp. (1994).

[36] W. H. Knox, D. S. Chemla G. Livescu, J. E. Cunningham, and J. E. Henry, "Femtosecond Carrier Thermalization in Dense Fermi Seas," Phys. Rev. Lett. **61**, 1290 – 1293 (1988).

[37] B. Braun, U. Keller, "Single frequency Q-switched ring laser with an antiresonant Fabry-Perot saturable absorber," Opt. Lett. **20**, pp. 1020 – 1022 (1995).

[38] S. A. Kutovoi, V. V. Laptev, S. Y. Matsnev, "Lanthanum scandoborate as a new highly efficient active medium of solid state lasers," Sov. J. Quantum Electr. **21**, pp. 131 – 132 (1991).

[39] B. Beier, J.-P. Meyn, R. Knappe, K.-J. Boller, G. Huber, R. Wallenstein, Appl. Phys. B **58**, 381 – (1994).